Vol 14 No 4, April 2005
1009-1963/2005/14(04)/0863-06

Chinese Physics

© 2005 Chin. Phys. Soc.
and IOP Publishing Ltd

Massive molecular cloud cores and activities of star formation*

Zhou Wu-Fei(周武飞)[a], Wu Yue-Fang(吴月芳)[a]†,
Wei Yue(魏 悦)[a], and Ju Bing-Gang(巨秉刚)[b]

[a] *Astronomy Department, Peking University, Beijing* 100871, *China*

[b] *Qinghai Station, Purple Mountain Observatory, De Ling Ha.* 817000, *China*

(Received 21 July 2004; revised manuscript received 13 December 2004)

We have mapped 23 sources in the J=1–0 lines of ^{12}CO, ^{13}CO and C^{18}O with the 13.7-m telescope at Qinghai station of Purple Mountain Observatory. The samples were chosen from the massive star formation regions whose single point lines have the broad-wing profile. The mapping shows that 12 clouds have cores and 5 outflows were identified with the ^{12}CO J=1–0 lines. Among the 12 cores, systematic velocity shifts were found in 2 cores, and blue asymmetric double-peak profile of ^{12}CO line was found in IRAS 19529+2704, indicating that it may be an infall candidate. Physical parameters of the cores and outflows were derived from the local thermodynamic equilibrium assumption. The masses range from $\sim 9.4\times10^2 M_\odot$ to $\sim 2.2\times10^5 M_\odot$. The hydrogen molecule densities range from $\sim 3.4\times10^2$cm^{-3} to $\sim 1.2\times10^4$cm^{-3}. The molecular outflows have masses larger than $3.5M_\odot$, and kinetic energies greater than 0.9×10^{38}J. The outflows have significantly greater masses and kinetic energies than those from low-mass young stellar objects (YSOs). For the cores, 2MASS data are available, dozens of 2MASS sources with different colour indices and brightness are often found around IRAS source, among which the reddest 2MASS source is always within the IRAS error ellipse thus probably corresponds to the IRAS source.

Keywords: Interstellar matter, molecular cloud, star formation
PACC: 9850E, 9840J, 9840, 9840C

The star formation and galaxy evolution are closely related to the formation of massive stars, due to their radiative, kinetic and chemical feedback into the interstellar medium. However, the formation of massive stars still remains poorly understood due to their scarcity and short evolution time scale. In addition, massive stars are usually born in clusters; hence their individual formation activities are difficult to resolve and study in detail, particularly because of their larger distances from the Sun than those of low-mass star formations. The earliest stages of massive stars are usually associated with hot molecular cores, H_2O maser, CH_3OH maser, molecular outflows and ultracompact H II regions (UCHII regions).[1] HII regions are useful tracers for high-mass star formation and O or B stars may have already formed in their centre recently. It is in these massive molecular cloud cores where new massive stars may be forming.

Although the CO molecular lines are not high-density tracers, we can use them to study the basic properties of the massive molecular cloud cores and their star formation activities, especially activities of large scale motions, for example outflow, rotation, and sometimes infall motion.

We have mapped 23 sources in the J=1–0 lines of CO and CO isotopes ^{13}CO, C^{18}O. The samples were chosen from Wu *et al*[2,3] and Wu *et al*,[4] mainly massive star formation regions associated with the H II region or H_2O maser and their CO or ^{13}CO J=1–0 lines having high-velocity wings in the single-point observation. All regions are associated with the Infrared Astronomical Satellite (IRAS) sources through a reference to IRAS PSC (IRAS Point Source Catalogue). Most of our mapping regions in the CO J=1–0 lines used the IRAS as reference position, and the rest used the maser position.

The CO, ^{13}CO and C^{18}O J=1–0 lines were observed with the 13.7-m telescope at the Qinghai sta-

*Project supported by the National Natural Science Foundation of China (Grant Nos 10133020, 10128306 and 10203003) and the National Key Basic Research Science Foundation (Grant No 1999075405).

†E-mail: yfwu@bac.pku.edu.cn

tion of Purple Mountain Observatory, during the period from January to December, 2003. The beam size at 112GHz is $106'' \times 70''$, the pointing and tracking accuracy is better than $10''$. The front end is an SIS (superconductor–insulator–superconductor) receiver, with which ^{12}CO and its isotopes, ^{13}CO and C^{18}O J=1–0 lines can be observed simultaneously. The noise temperature of the system, including the atmosphere at zenith, was 250K (single side-band). The acousto-optical spectrograph (AOS) has 1024 channels and its total bandwidth is 145.43MHz for ^{12}CO, 42.87MHz for ^{13}CO, and 43.3MHz for C^{18}O, respectively. The spectral resolution is 209kHz for ^{12}CO, 78.7kHz for ^{13}CO, and 75.7kHz for C^{18}O, respectively. The antenna temperature $T_{\rm A}^*$ was calibrated with the atmospheric temperature and corrected for atmospheric absorption, antenna cover loss, radiator loss and rearward scattering and spillover. The radiation temperature is calculated by $T_{\rm R} = T_{\rm A}^*/\eta_{\rm MB}$, where $\eta_{\rm MB}$ is the antenna main beam efficiency. For our source, $\eta_{\rm MB}$= 42% at 112GHz. The system noise level was 0.26K at 209kHz resolution with an on source integration time of 60s. For the mapping observations the absolute position switch mode was used. The map size was usually $5' \times 5'$ with a step of $1'$ except some sources marked by * in Table 1, whose α (right ascension in equator coordinate system) step was $1' \times \cos\delta$ due to the previous observation program, where δ is the declination of these sources. Then if the line was still strong enough on the border of the map, mapping was extended until the line intensity reached less than or equal to half of the maximum value.

We analysed the spectral lines, calculated the emission intensity and made contours. For sources with high- velocity wings, we identify the outflows from the position–velocity (P–V) diagram after excluding other supersonic motions. The J=1–0 emission of ^{12}CO, ^{13}CO and C^{18}O were detected in all the 23 sources, but only in two sources, IRAS 06055+2039 and IRAS 19282+1814, C^{18}O were strong enough for analysing core properties. The results show that there are cores in 12 sources, outflows in 5 cores, systematic velocity shifts in 2 cores, and blue asymmetric double-peak profile of ^{12}CO line in 19529+2704 which indicates that there may be infall motion.[5–7] An example for cloud core, outflow, systematic velocity shift and blue line profile are shown in the figure below. Three sources, namely IRAS 18507+0110, 19291+1713 and 20281+4038 have multiple emissions, and are not suitable for analysing star formation activity; six sources have more than one component, their main component was chosen for analysis; and two sources, IRAS 19282+1814 and K47 have cores which can be found in Wu *et al*,[4] but did not display full cores in our result due to the smaller mapping areas.

Table 1. Core parameters. Column 3 is the dynamical distance D calculated by the observed line centre velocity of ^{12}CO,[9] except IRAS 06067+2138, whose distance is quoted from Ref.[10]. Column 4 is the excitation temperature calculated by the peak antenna temperature $T_{\rm A}^*$ of ^{12}CO.[11] In columns 5–7 are listed $\Delta V_{\rm FWHM}$, optical depth and the average column density of ^{13}CO within the core area, respectively. The major and minor angular size a and b were taken from the contour at about half of the maximum, and the linear size $R = \sqrt{ab}/2$. They are shown in columns 8–10, respectively. The density of hydrogen molecules is listed in column 11 and the core mass in column 11. Column 13 is the virial mass calculated using the $\Delta V_{\rm FWHM}$ and the linear size R.[12] The last column is the bolometric luminosity of the reference IRAS source calculated from the PSC flux data.[13]

Source	Ref. Position	D	$T_{\rm ex}$	$\Delta V_{\rm FWHM13}$	τ_{13}	$N_{^{13}{\rm CO}}$	A	b	R	$n_{\rm H2}$	M	$M_{\rm vir}$	$L_{\rm bol}$
	J2000	/kpc	/K	/km·s^{-1}		/10^{15}cm^{-2}	/arcmin	/arcmin	/pc	/10^3cm^{-3}	/$10^3 M_\odot$	/$10^3 M_\odot$	/$10^3 L_\odot$
(1)	(2)	(3)	(4)	(5)	(6)	(7)	(8)	(9)	(10)	(11)	(12)	(13)	(14)
00420+5530	$00^{\rm h}44^{\rm m}57.5^{\rm s}$ $+55^{\rm d}47^{\rm m}18^{\rm s}$	5.0	22	1.9	0.38	14	4	2.5	2.3	0.90	8.9	1.7	16
05335+3609	$05^{\rm h}36^{\rm m}52.5^{\rm s}$ $+36^{\rm d}10^{\rm m}49^{\rm s}$	15	19	4.0	0.46	31	5	2.5	7.8	0.57	223	26	20
06055+2039	$06^{\rm h}08^{\rm m}32.8^{\rm s}$ $+20^{\rm d}39^{\rm m}16^{\rm s}$	2.4	44	3.9	0.49	130	5	7	2.1	9.0	41	6.7	16
06067+2138	$06^{\rm h}09^{\rm m}48.0^{\rm s}$ $+21^{\rm d}38^{\rm m}11^{\rm s}$	2.0	19	2.4	0.72	23	3	3	0.88	3.7	2.1	3.4	0.35
06446+0029*	$06^{\rm h}47^{\rm m}12.9^{\rm s}$ $+00^{\rm d}26^{\rm m}06^{\rm s}$	6.0	18	2.2	0.18	4.9	2	1.5	1.5	0.47	1.8	1.5	23
19120+0917	$19^{\rm h}14^{\rm m}23.7^{\rm s}$ $+09^{\rm d}23^{\rm m}14^{\rm s}$	4.1	14	3.6	0.67	18	3	2	1.5	1.7	3.5	4.0	40
19529+2704*	$19^{\rm h}54^{\rm m}59.7^{\rm s}$ $+27^{\rm d}12^{\rm m}52^{\rm s}$	3.4	24	2.6	0.35	25	2	3	1.4	2.6	6.7	2.0	39
		4.0	24	2.6	0.35	25	2	3	1.1	3.2	4.6	1.7	56
20100+3643*	$20^{\rm h}11^{\rm m}54.1^{\rm s}$ $+36^{\rm d}52^{\rm m}28^{\rm s}$	4.2	15	3.4	0.29	8.2	1.5	1.5	0.94	1.2	0.94	2.2	7.0
21074+4949*	$21^{\rm h}09^{\rm m}07.9^{\rm s}$ $+50^{\rm d}02^{\rm m}00^{\rm s}$	9.5	17	3.5	0.2	5.9	2	1.5	2.4	0.35	5.6	6.3	84
		9.8	17	3.5	0.2	5.9	2	1.5	2.5	0.34	5.9	6.1	89
22570+5912*	$22^{\rm h}59^{\rm m}06.5^{\rm s}$ $+59^{\rm d}28^{\rm m}28^{\rm s}$	5.0	35	3.3	0.33	54	2	3	1.8	4.4	24	4.2	48
23504+6012	$23^{\rm h}52^{\rm m}58.2^{\rm s}$ $+60^{\rm d}28^{\rm m}44^{\rm s}$	4.0	23	2.6	0.33	18	2.5	4	1.6	1.6	6.8	2.3	8.2
S157	$23^{\rm h}16^{\rm m}04.3^{\rm s}$ $+60^{\rm d}01^{\rm m}41^{\rm s}$	4.4	32	2.9	0.27	27	2	5	2.0	1.9	11	3.6	85

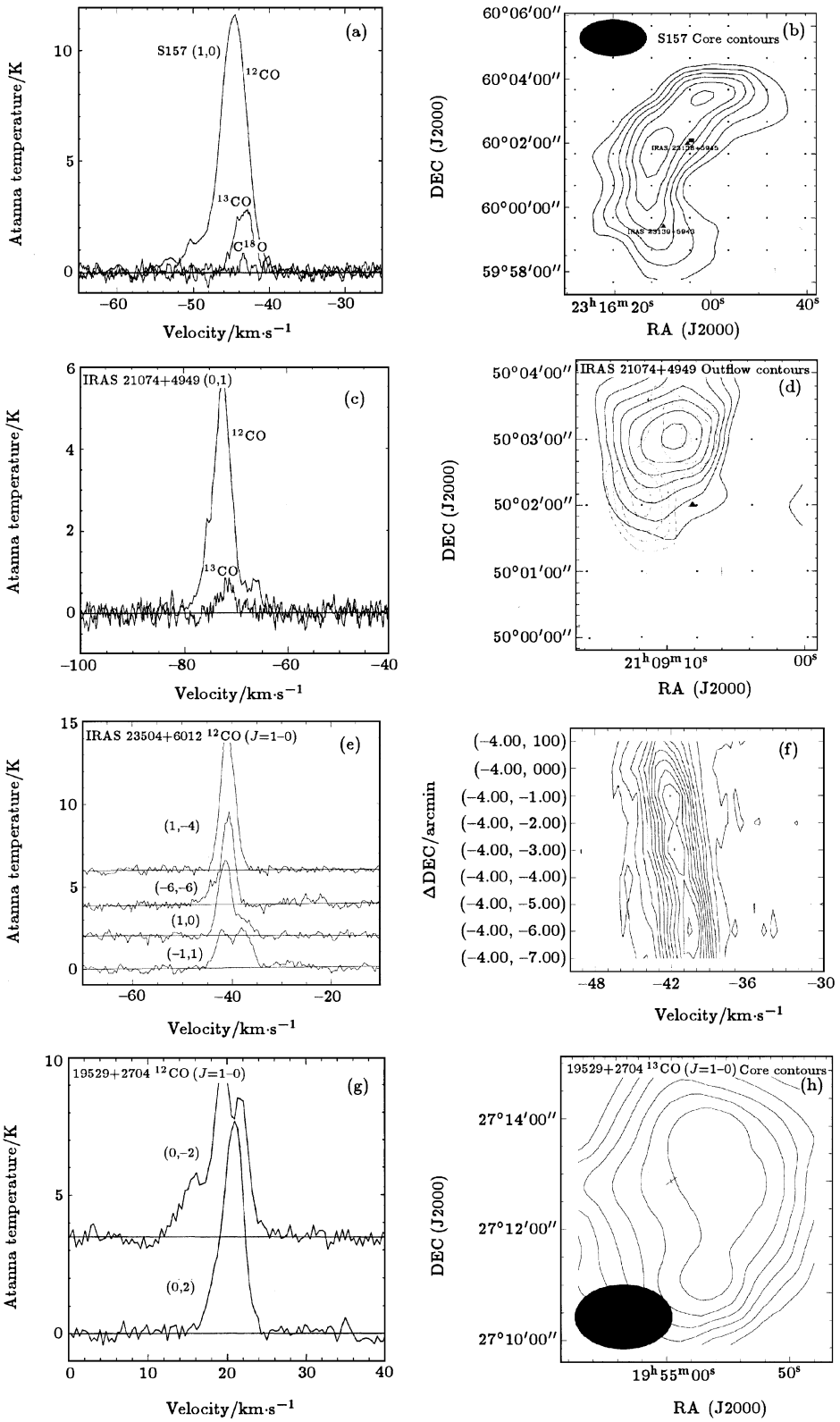


Fig.1. Examples of spectral lines, core, outflow, rotation and infall: (a) ^{12}CO, ^{13}CO, C^{18} O spectral lines of S157 offset (1, 0). (b) Contours of ^{13}CO emission from –46.0 to –40.8km·s^{-1}. Contours are at 8, 10, 12, 14, 16, 18K km·s^{-1}. The square denotes the HII region, the cross denotes the H_2O maser source, the triangle denotes the IRAS source and the shaded ellipse shows the beam size. (c) ^{12}CO, ^{13}CO spectral lines of IRAS 21074+4949 at offset (0, 1). (d) Blueshifted ^{12}CO emission contours from –81.1 to –75.3 km·s^{-1}(solid lines) and redshifted emission contours from –69.2 to –62.1 km·s^{-1} (dashed lines). All contour levels begin from 3K km·s^{-1} with increasing steps of 1.0K km·s^{-1}. The cross denotes the H_2O maser source and the triangle denotes the IRAS source. (e) The ^{12}CO spectral line of the IRAS 23504+6912 at offset (1, –4) (–6, –8), (1,0) and (–1,1), respectively. (f) Position–velocity contours graph of 23504+6012. The contour levels begin from 0.4 K with increasing steps of 0.6 K. (g) The ^{12}CO spectral line of the19529+2704 at offset (0, –2) and (0, 2), respectively. (h) Contours of ^{13}CO emission integrated from 19.3 to 23.5 km·s^{-1}, contour levels from 7.3 to 14.8 with steps of 1.4K km s^{-1}.

Assuming that the gas is in local thermodynamic equilibrium (LTE)[8] and taking the molecular abundance ratio of $[^{12}CO]/[^{13}CO]$=89, we can calculate the excitation temperature of ^{12}CO and the optical depth of ^{13}CO with the radiation transfer theory. And assuming that the peak optical depth of ^{13}CO is the average optical depth of the area, we can calculate the average column density of ^{13}CO with the optical-depth correction. Taking the molecular abundance ratio $[^{12}CO]/[H_2]=1\times10^{-4}$, the parameters of the whole molecular cloud core, whose the most abundant component is H_2, can also be derived. The main derived parameters and some observed parameters of cores are listed in Table 1.

The emission of ^{13}CO and $C^{18}O$ J=1–0 shows that the gas in these sources is cold and dense. The excitation temperature of ^{12}CO ranges from ∼15 to ∼43 K, the average column density of ^{13}CO is $\sim(5–130)\times10^{15}cm^{-2}$, and the average numeral density of H_2 of the core areas is $\sim(0.35–12)\times10^3cm^{-3}$.

It has been shown that emission line widths of massive cores are often greater than those of low-mass cores, according to Wu *et al*[14] and the references quoted therein. The typical line width of ^{13}CO J=1–0 is 1.3km·s^{-1} for the low-mass cores in the surveys of Myers *et al.*[15] Of our 12 cores, 7 have ^{13}CO J=1–0 line widths greater than 3.0km·s^{-1}, 4 have line widths greater than 2.5km·s^{-1}, the last one IRAS 00420+5530 only has 1.9km·s^{-1} line width. Among the 12 cores, 11 cores have one or more IRAS sources having bolometric luminosity $L_{bol} > 10^3L_\odot$, indicating that they should have high-mass young stellar objects (YSOs).

We also calculated the virial mass (M_{vir}). Assuming a constant density distribution that can give an upper-limit to our estimation of virial mass, the virial mass is given by[12] $M_{vir} = 210R\Delta V^2$ ($M_\odot$), where R measured in pc (parsec) is the cloud core radius and ΔV measured in km·s^{-1} is the full width at half-maximum (FWHM) intensity of ^{13}CO J=1–0 line in the present paper. Comparing the core masses with their virial masses, we can estimate if the cores are unstable for the gravitational collapse. In 8 cores the masses are greater than their virial masses, indicating that they are the star forming regions indeed. For the remaining 4 cores whose masses are less than their virial mass, there may be some unstableness in the cloud cores.[12]

An estimate of the outflow parameters was also obtained, following the method used by Snell *et al.*[16] Similarly assuming the high-velocity gas being in LTE and optically thin, the total column density of high-velocity gas can be obtained. With the area of the red and blue lobes, the mass M can be deduced. In a similar way, the momentum and energy can be calculated from the summation of $\int T(v)v\mathrm{d}v$ and $\int T(v)v^2\mathrm{d}v$ over the lobes, respectively. A characteristic velocity can be determined by $< V >= P/M$, and dynamical time scale got by $t = R/V_{max}$, the driving force and mechanical luminosity by $F = P/t$, $L_{co} = E/t$, and the stellar mass loss rate by $\dot{M} = P/(t \cdot V_w)$, where the terminal velocity of the stellar wind V_w is taken to be 1000km/s.[17] In addition, we give a uniform inclination of 45° to the velocity $< V >$ to correct for the projection effects. The results are presented in Table 2.

Table 2. Outflow parameters. Column 2 is the typical ΔV_{FWHM} of ^{12}CO. Column 3 lists the blue or red lobe, and if the dynamical distance D have two values, the related parameters are calculated twice for the different D. The parameters of outflows are listed in columns 4–12, respectively.

source	ΔV_{FWHM12} /km·s^{-1}	Lobe	R /pc	M /$M_\odot$	P /$M_\odot$km·s^{-1}	E /10^{38}J	$< V >$ /km·s^{-1}	t_d /10^5yr	F /$10^{-5}M_\odot$km·s^{-1}yr^{-1}	L_{co} /$L_\odot$	$\dot{M}$ /$10^{-7}M_\odot$ yr^{-1}
00420+5530	3.08	Blue	2.0	42	180	6.1	4.3	3.3	5.5	0.15	5.5
		Red	2.0	29	156	7.0	5.5	3.2	4.9	0.18	4.9
20100+3643	4.15	Red	0.53	3.5	21	0.90	6.0	0.75	2.8	0.10	5.6
19529+2704	5.50	Red near	1.2	7.1	68	5.1	9.7	1.3	5.2	0.31	5.2
		Red far	1.4	9.7	100	7.4	9.7	1.6	6.2	0.37	6.2
21074+4949	4.52	Blue near	1.6	22	168	9.9	7.8	1.9	8.7	0.42	8.7
		Blue far 1.7	23	177	11	7.8	2.0	9.0	0.43	9.0	
		Red near	1.6	17	184	15	11	1.5	12	0.8	12
		Red far	1.7	18	196	19	11	1.6	13	0.82	13
S157	4.15	Red	0.76	21	197	14	9.3	0.75	26	1.6	26

Our outflow parameters are significantly larger than those produced by low-mass YSOs. We find the mass in the single lobe of outflows ranges from 3.5 to 42.3 $M_{\odot}$, momentum P=21 to 79 $M_{\odot}$km·s^{-1}, mechanical energy E=9×10^{37} to 1.6×10^{39}J and stellar mass-loss rate $\dot{M}$ = 4.9 × 10^{-7} to 2.6×10$^{-6}M_{\odot}$yr^{-1}, much larger than those found for low-mass outflows. Among the 5 outflows, three outflows which only show red lobe parameters are not monopolar outflows because their blue side is polluted by the other components.

Systematic velocity shift was found in 2 sources IRAS 20100+3643 and 23504+6012. The core region is only shown partly for IRAS 20100+3643, and there is high-velocity molecular gas in the core region. The velocity gradient from north to south is 0.29km·s^{-1}pc^{-1}. A rotation with angular velocity 9.3×10^{-15}s^{-1} can account for it. For IRAS 23504+6012 the velocity gradient from north to south is 0.30km·s^{-1}pc^{-1}, and a rotation with angular velocity 9.8×10^{-15}s^{-1} can account for it. There are some line wings in the ^{12}CO J=1–0 lines of the two sources.

We also found blue asymmetric double-peak profiles of ^{12}CO lines in the core of IRAS 19529+2704. The line positions are associated with the core contour intensity peak and about 2′ south away from the IRAS 19529+2704, which is larger than the beam width and out of the IRAS ellipse of error. In Fig.1(g), we can see that a line of offset (0, 2) is single-peaked obviously and its line-center velocity is exactly at the dip position of the line at position of offset (0, –2). The collapse demands that the optical-thin line has a single peak at the corresponding position of the double-peak optical-thick line.[18] But our ^{13}CO lines have a little similar blue asymmetric double-peak profile, indicating that it may be somewhat optical-thick for the ^{13}CO, and the S/N ratio of C^{18}O is not enough to ascertain if the C^{18}O lines have a single-peak feature. So this source needs more sensitive and higher space resolution observations with dense environment molecular probes such as HCN, HCO^{+} and optical-thin lines.

The 2MASS data were employed and the local stars of 2MASS sources are removed. Most of our IRAS sources in the 12 cores can find correspondence in 2MASS sources within their IRAS error ellipse. There is often not only one 2MASS source in the IRAS error ellipse, for example, the IRAS 19529+2704 has 5 2MASS sources within its IRAS error ellipse and 52 2MASS sources within 1′ region centered at the IRAS source position, which indicates that massive stars are often formed in clusters. However, we can always find a red bright source corresponding to the IRAS source. For example, 2MASS J19545807+2711589, whose JHK magnitudes are 16.2, 14.0 and 12.9, respectively, coincides with IRAS 19529+2704. An infrared cluster locates in the northern part of the CO core (see Fig.1(h)); while the southern part is dark in both 2MASS and POSS images. Thus the star formation is occurring from north to south. 2MASS J19545807+2711589(or 2MASS J19545807+2711589), about 30 arcsec from the cluster, at the interface of the two parts, is really young.

The reference position of S157 cloud core locates about 5 arcmin south-west to the HII region.[19] Its 2MASS image shows that there is a small bar-like infrared cluster wedging into the molecular cloud from south-west. The CO cloud core emission peak is about 1 arcmin east to the reference position, IRAS 23138+5945.

The 12 cloud cores in our sample are very young in general. They are associated with IRAS sources whose colour indices satisfied the criteria of UCHII region.[20] Eight sources are associated with water masers.[21,22] Their masses range from several hundreds to tens of thousands of solar mass. Most ^{13}CO line widths at half maximum intensity are larger than or close to 3km·s^{-1}.[23] All these above indicate that these cloud cores are possible massive star formation regions. Among the five outflow sources, gravitational collapse may be ongoing in IRAS 19529+2704 and the spectra in IRAS 20100+ 3643 and 23504+6012 show the characteristics of rotation. All are the important dynamic processes of star formation.

In summary, 23 sources have been mapped in the J=1–0 transition of ^{12}CO, ^{13}CO and C^{18}O and analysed for star formation activities. Twelve cores and 5 outflows were identified as our result. These cores and outflows are mostly massive ($M_{\rm core}$=10^3−10$^5M_{\odot}$, $M_{\rm outflow}$ = 3.5 − 42$M_{\odot}$) and mostly associated with high bolometric luminosity ($L_{\rm bol}$ = 10^3 − 10$^5L_{\odot}$) IRAS sources. In addition, two rotational cores and an infall candidate were found in these high mass cores. The line widths of 10 massive cores are greater than 2.5km·s^{-1}, obviously greater than the line width of low-mass cores. And the 2MASS data indicate that the massive star formation region often has several or dozens of infrared sources within it.

Future high-resolution observations in multiple molecular lines and IR imaging are required to locate the central driving engine and determine if more than

one outflow exists within our telescope beam.

We wish to thank the staff of Qinghai Station Purple Mountain Observation for their assistance in the observations. This research has made use of the NASA/ IPAC Infrared Science Archive, which is operated by the Jet Propulsion Laboratory, California Institute of Technology, under contract with the National Aeronautics and Space Administration.

References

[1] Henning Th, Schreyer K, Launhardt R and Burkert A 2000 *Astron. Astrophys.* **353** 211
[2] Wu Y, Li Y and Zheng L 1998 *Astron. Astrophys. Chin.* **22** 459
[3] Wu Y *et al* 1998 *Acta Astrophys. Sin.* **18** 415
[4] Wu Y, Wu J and Wang J 2001 *Astron. Astrophys.* **380** 665
[5] Walker C K, Lada C J, Young E T, Maloney P R and Wilking B A 1986 *Astrophys. J.* **309** L47
[6] Zhou S 1992 *Astrophys. J.* **394** 204
[7] Zhou S 1995 *Astrophys. J.* **442** 685
[8] Lada C J 1985 *Ann. Rev. Astron. Astrophys.* **23** 267
[9] Wouterloot J G A and Brand J 1989 *Astron. Astrophys. S.* **80** 149
[10] Carpenter J M, Snell R L and Schloerb F P 1995 *Astrophys. J.* **450** 201
[11] Sato F *et al* 1994 *Astrophys. J.* **435** 279
[12] MacLaren I, Richardson K M and Wolfendale A W 1988 *Astrophys. J.* **333** 821
[13] Casoli F *et al* 1986 *Astron. Astrophys.* **169** 281
[14] Wu Y, Wang J and Wu J 2003 *Chin. Phys. Lett.* **20** 1409
[15] Myers P, Linke R A and Benson P J 1983 *Astrophys. J.* **264** 517
[16] Snell R L, Scoville N Z, Sanders D B and Erickson N R 1984 *Astrophys. J.* **284** 176
[17] Lamers H J G L M, Snow T P and Lindholm D M 1995 *Astrophys. J.* **455** 269
[18] Snell R and Loren B 1977 *Astrophys. J.* **211** 112
[19] Israel F P 1980 *Astron. J.* **85** 1612
[20] Wood, D O S and Churchwell E 1989 *Astrophys. J.* **340** 265
[21] Comoretto G *et al* 1990 *Astron. Astrophys. Suppl.* **84** 179
[22] Brand J *et al* 1994 *Astron. Astrophys. Suppl.* **103** 541
[23] Wu Y, Wang J and Wu J 2003 *Chin. Phys. Lett.* **20** 1409